TURKISH JOURNAL OF REMOTE SENSING
(Türkiye Uzaktan Algılama Dergisi)
e-ISSN 2687-4997
https://dergipark.org.tr/en/pub/tuzal

Visualization of M3C2 outputs obtained from an open pit mine field

Mehmet Güven Koçak[1], Nilüfer Özdaş[2], Osman Sami Kırtıloğlu[*3]

[1] *Izmir Katip Celebi University, Faculty of Engineering and Architecture, Department of Geomatics Engineering, Cigli, İzmir, Türkiye;* mehmetguven.kocak@ikcu.edu.tr
[2] *Izmir Katip Celebi University, Faculty of Engineering and Architecture, Department of Geomatics Engineering, Cigli, İzmir, Türkiye;* nilufer.ozdas@ikcu.edu.tr
[3] *Izmir Katip Celebi University, Faculty of Engineering and Architecture, Department of Geomatics Engineering, Cigli, İzmir, Türkiye;* osmansami.kirtiloglu@ikcu.edu.tr

Article History:
Received: 17 April 2025
Revised: 10 May 2025
Accepted: 30 May 2025
Published: 30 December 2025

Abstract: Open pit mining is a common technique for extracting surface mineral resources, but it poses safety risks due to terrain instability and slope movements. Accurate and efficient monitoring of surface changes is essential for operational safety and informed decision-making. Recently, UAV-based photogrammetric point clouds have emerged as a cost-effective and flexible alternative to traditional geodetic methods. Among the analysis tools, Multiscale Model to Model Cloud Comparison (M3C2) stands out for detecting 3D changes between epochs. However, standard M3C2 relies on internal accuracy, which may lead to overly optimistic assessments. This study introduces a visualization-based approach using realistic external-accuracy test statistics derived from GNSS control points. Within the approach, a new visualization metric based on the ratio of the norms of 2D and 3D change vectors is proposed. In cases where there is a predominant movement in the horizontal direction, the calculated ratio values are larger compared to their immediate surroundings. In this way, these locations become more perceptible and user attention is directed to the highlighted locations. Thus, it will be possible especially for non-specialized users to better examine these prominent locations in the images and in the field when necessary. In this way, decision makers will be provided with a practical tool to alert the field personnel working in the relevant locations and to ensure security quickly. The findings show that visualization supported by realistic accuracy values can significantly contribute to the identification of landslide areas that may be caused by excavation and are likely to progress over time in an open pit mine site.

Keywords: Open pit mining; M3C2 algorithm; 3D change detection; UAV photogrammetry; spatial visualization

Citation: Koçak, M.G., Özdaş, N., & Kırtıloğlu, O. S. (2025). Visualization of M3C2 outputs obtained from an open pit mine field. *Turk. J. Remote Sens.*, 7(2), 218-231. https://doi.org/10.51489/tuzal.1677755

1. Introduction

In recent years, open pit mining has increased significantly due to its economical and flexible nature for the extraction of young, near-surface deposits. These surface mining sites offer a low-cost production environment to meet the growing energy demand of societies. Many countries also support this sector for its advantageous income generating potential. In addition to the economic benefits, open pit mining provides safer working environments for workers than underground mining (Altiti et al., 2021). As with any operation, open pit mining is not risk-free and involves certain risks. Mass displacements may occur because of gravity during excavations. Especially in areas where the slope of the topography is high, excavation in the lower elevated locations may trigger a downward movement of the mass in the upper elevations. Determining whether this movement has begun and where it has been occurring is an important safety need for the workers and for the prevention of material damage.

To improve the quality and efficiency of the mining site operations as well as to plan, coordinate, and manage these operations, spatial data collection should be carried out at regular time intervals. In the not-too-distant past, when technology was not widespread and more costly to access, the interval for laborious data collection was set longer. However, low-

cost imaging devices and carrying platforms have enabled prompt and flexible data acquisition. Easily obtainable data allows undertaking more frequent monitoring activities at the site. This has improved the effective management capacity of the mine field by maintaining strict safety controls.

Various spatial products can be utilized to ensure safety in mine sites. For example, risk maps can be produced to present landslide susceptibility. These maps show the risk value at a location obtained by combining different attribute data of the area under a multi-criteria decision-making algorithm. However, these maps have been prepared using small-scale topographic maps and they exhibit the risk only in general terms. Security monitoring depending solely on the risk maps will not meet the standards for constantly changing, dynamic environments as in open pit mining.

In open pit mine operations, monitoring change and safety go hand in hand and cannot be separated from each other. Here, data must be up-to-date and continuous. Historically, data acquisition quality and density has changed significantly over time in parallel with technological developments. While systems were initially designed to deliver sparsely distributed point data, modern systems provide opportunistic and dense data acquisition that better represent the surface. For example, geodetic surveying instruments (total station, level, GNSS-RTK etc.) capture point data with an accuracy of cm or less. The resulting geodetic dataset shows a sparse and inhomogeneous point distribution. However, monitoring surface changes demand more dense point sets as in the case of open pit mines. Photogrammetric systems enable acquiring dense point clouds and the distribution of these points can be more homogeneous compared to geodetic systems. In recent years, drone-mounted cameras and LiDAR systems are frequently used for surface data collection. Practitioners prefer camera systems over LiDAR in terms of cheaper operation in the field.

Geodetic data collection is a time-consuming operation, and the topography may challenge and expose the survey team to several on-site risks. Drones suit well for mapping inaccessible areas in a short period of time and make data acquisition more secure than terrestrial geodetic systems. Despite their disadvantages, practitioners still benefit from geodetic systems for georeferencing and model validation purposes.

The spatial data needed for monitoring and management of activities in mining areas can be acquired in the most cost-effective way by producing photogrammetric point clouds with the help of drones (Ren et al. 2019). The point cloud is converted into a digital elevation model (DEM) through meshing, interpolation and filtering stages, and the change can be revealed by comparing two DEMs of successive epochs. In this method, known as DEM of Difference (DoD), only the change in the vertical direction can be analyzed with the constraint that the components in the horizontal direction are constant. However, the change can also be revealed by comparing the raw point clouds. Multiscale Model to Model Cloud Comparison (M3C2) is a widely accepted method based on the principle of directly comparing point clouds without any additional processing (Lague et al., 2013). Unlike DoD, M3C2 calculates the 3D change vector by comparing point cloud data belonging to two different epochs.

In most of the studies using M3C2, the results are presented and interpreted visually (Lague et al., 2013; Cook, 2017; Liu et al., 2023; He et al., 2024). Yan et al (2024) monitored the changes before and after rainfall at different slope locations in a catchment area using four different methods, including the M3C2 algorithm, with UAV-integrated photogrammetric and laser systems. They incorporated visualization to qualitatively assess their results. Regardless of the methods used for change analysis several studies emphasize the importance of visualization. For example, Teng et al (2022) suggested to use VR/AR tools for visualization of point clouds and to conduct further research on this topic. Song et al. (2024) examined the current state of early warning systems in mine sites. They discussed the visualization capacities of these systems as a whole and underlined the basic need of visualization for better presenting spatial data in GIS environment.

As in many fields, machine learning applications have been deployed in geosciences (Reichstein et al., 2019). In the field of mining, machine learning is used to understand complex geological and geotechnical phenomena and to improve decision-making processes with big data solutions (Liang et al., 2023). For example, machine learning is utilized in solving slope stability problems that may be encountered in open mine applications (Ospina-Dávila et al., 2020; Hacıefendioğlu et al., 2021). Although machine learning and AI solutions have been incorporated into many fields, the takeover of all jobs by AI in the modern sense has not yet been realized. Here, human capacity remains superior, especially in situations of uncertainty encountered in decision-making applications and in situations where skills such as creativity and interpretation need to be used (Jarrahi, 2018). Especially in emergency situations that require immediate intervention, human cognitive capacity may need to be used. Forecasting the precise timing of slope failures remains challenging and is an active area of research (Intrieri et al., 2019). However, the large size and diversity of data necessitates decision makers to select and extract the necessary information depending on its relevance to the subject under investigation. Here, human attention should be directed to the selected information and unnecessary ones should be ignored (Carrasco, 2011). In this context, visualization is still an important tool for decision makers and should be used effectively.

This study aims to visualize M3C2 output as a decision support in a mine site where excavation areas are dominant, but landslide locations are also observed. Instead of the 1D test statistic adopted by M3C2, which is based on the determination of significant change vectors using internal accuracy criteria, an external accuracy-based 3D test statistic is used. A visualization-based approach is proposed to spot locations where landslides occurred, and potential ones could occur. In this way, visual materials produced at a less computational cost can be used in quick decision-making situations.

2. Materials and Methods

In this study, we did not collect any data in the field but used readily available data obtained by the company of an open-cast coal mine site. The study area is between 39°.1236–39°.1354 N latitudes and 27°.5730–27°.5944 E longitudes, within the boundaries of Soma district in Manisa province, Türkiye. The site is located approximately 57 km northeast of Manisa and 5 km southwest of Soma city centers. The mining site has elevation ranges between 680 and 865 meters above mean sea level with rolling topography. The open-pit mining area covers a total of 2.4 km^2 (Figure1). Within the scope of mining activities, the lignite ore extracted from the study area is located within the Miocene-aged marl formation and is classified as Group 4 lignite according to Türkiye's coal classification system. The mining operations are conducted using mechanical excavation methods without blasting. The ore is extracted by excavators and transported by trucks. The extracted ore is stored in stockpiles within the site, while waste materials are deposited as spoil heaps.

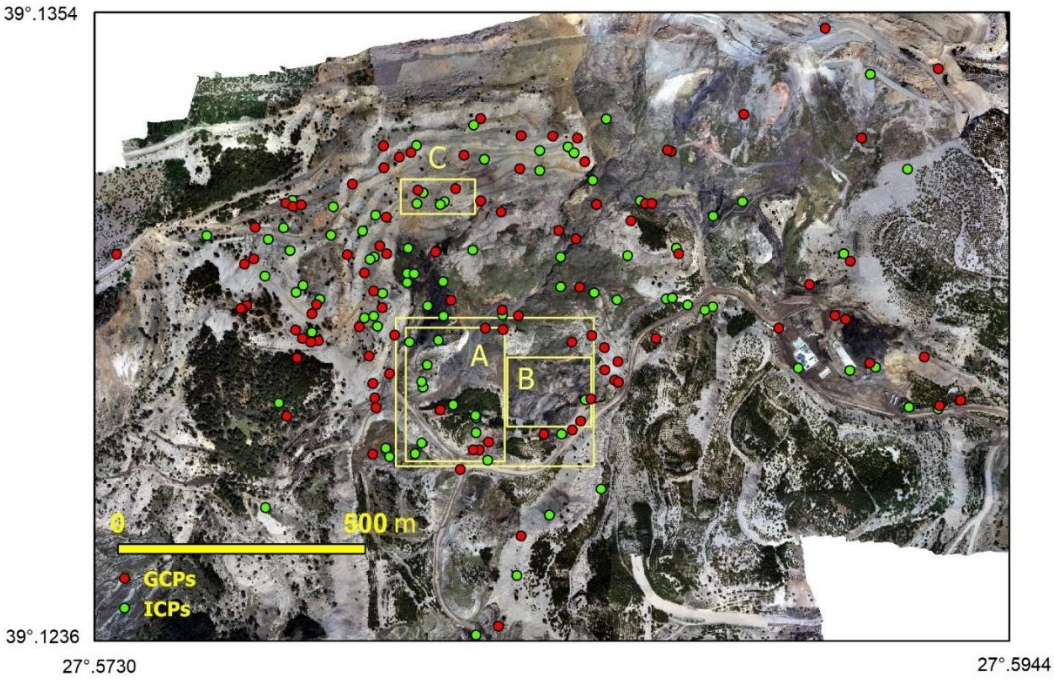

Figure 1. Study area having dimensions of 1.3 x 1.8 km extension. Colored circles denote GCP and ICP locations used in the field at ten different epochs. Note that not all GCPs and ICPs were used in each measurement epoch, but only a subset of these within the imaged area (cf. Table 2)

Surveying data in the study area were obtained in 10 surveying epochs over 19 months by the company operating the mine site. The Turkish General Directorate of Mining and Petroleum Affairs (MAPEG) demands the mining companies to prepare production plans and to monitor production areas dynamically (MAPEG, 2025). In this context, the company performed terrestrial and photogrammetric measurements at irregular time intervals depending on the development of excavation works in the site. In each epoch, imaging was performed not in the entire site but in the areas where changes occurred due to excavation. Therefore, the number of images is obtained differently from epoch to epoch. As can be seen in Table 1, the flight altitudes and average ground sampling intervals of the images taken at different epochs may also differ due to imaging various distinct topography.

The dataset used in the study includes data collected in 10 different epochs (Table 1). Initial epoch (Epoch 0) was collected on 27.03.2021 and Epoch 9 was collected on 19.10.2022. The time periods between successive epochs are not uniform, and the shortest interval is seen between Epoch 4 and Epoch 5 with 10 days, while the longest time interval is 160 days between Epoch 7 and Epoch 8. All imagery is captured using a DJI Phantom UAV with the FC6310S camera model having focal length of 8.8 mm and pixel size of 2.41 μm. The numerical data of the flights are presented in Table 1.

Agisoft Photoscan was used to acquire point clouds (Agisoft LLC, 2018). The software performs two-stage photogrammetric orientation of the images to reconstruct the surface. In the first stage, sharp details in the images are extracted and matched. The second stage consists of a bundle block adjustment model using the image coordinates of the homologous points acquired in the first stage. Here each measured image coordinate is modeled as a function of parameters such as interior, exterior orientation elements, and 3D object coordinates. Ground control points (GCPs) are introduced to remove the rank deficiency of the model; thus, they define the datum of the system. The least squares method is applied to the bundle block model and its parameters are estimated together with model deviations which are in turn used to compute quality measures. Apart from internal model deviations independent control points (ICPs) are used for a more realistic model validation.

Table 1. UAV campaign data

Epoch	Days from Previous Epoch	Total Images	Altitude (m)	Mean Ground Sampling Distance (GSD) (cm)	Area (km²)
Epoch 0 March 27, 2021	0	450	168	6.6	1.490
Epoch 1 May 30, 2021	64	375	239	6.5	1.010
Epoch 2 June 23, 2021	24	352	208	5.6	1.750
Epoch 3 Aug. 2, 2021	40	401	245	6.8	1.820
Epoch 4 Aug. 23, 2021	21	454	212	5.5	0.772
Epoch 5 Sep. 2, 2021	10	278	228	6.2	0.587
Epoch 6 Oct. 1, 2021	29	433	198	5.3	0.636
Epoch 7 Nov. 6, 2021	36	295	215	5.9	0.470
Epoch 8 April 15, 2022	160	592	202	5.8	2.440
Epoch 9 Oct. 19, 202	156	570	220	6.0	2.910

Change in mining activities can be determined by taking the difference of digital elevation models obtained for two epochs. In this method, known as DEM of Difference (DoD), the point clouds obtained for each date must be converted into a digital surface/terrain model. Although DoD is advantageous in applications that require ease of calculation and rapid detection of changes over large areas, it is not a suitable method for vertically extending objects where the surface to be examined cannot be represented by a digital surface model (Lague et al., 2013). In addition, only changes in the vertical direction can be revealed by comparing horizontally oriented grids within DoD. Therefore, the change is presented here in one dimension. However, it may be preferable to perform 3D change analysis in problems where the change is dynamic.

Among others, M3C2 is the widely used 3D analysis method where it compares point clouds obtained at two distinct epochs. The method works in two stages and uses plane and cylinder as auxiliary surfaces for the solution (Lague et al., 2013; Özdaş et al., 2024). In the first stage, for each point in the reference cloud a plane is estimated with the help of the points lying in the D diameter neighborhood of this point and its normal direction is calculated. In the second stage, the intersection of the reference and comparison point clouds is taken with a cylinder of radius d/2 passed along the estimated normal direction. All points lying within the cylinder are projected to the normal direction. The coordinate centers of these projection points are found separately both for the reference and the compare sets. The two coordinate centers in the normal direction are the start and end points of the change vector. Its direction is from the reference set to the comparison set and its norm is the amount of change.

In the study, CloudCompare v2.12.2 software was used to obtain the change between two epochs as a 3D changing vector using point clouds (CloudCompare, 2020). The raw point clouds loaded into the program were processed through the M3C2 distance plugin. M3C2 delivers three coordinate values for each point in the reference cloud, change vector norm, and three-unit vector components of the change vector. In addition to these seven parameters, M3C2 also calculates variables related to the quality of the solution for each reference point. These variables are the number of points within the boundaries of the cylinder with diameter d for both clouds, the standard deviation value of change vector norm, and an indicator value (0/1: insignificant/significant) that shows the statistical significancy of the norm.

3. Visualization

Raw data can be subjected to various analyses and used to extract information from simpler to more complex levels. Various algorithms and models are utilized in the evaluation of data. For example, a bundle block adjustment model based on the collinearity equation is used to obtain a digital elevation model from photogrammetric images. Other derived quantities such as slope and aspect can be extracted from the digital elevation models. The

DEM and other derived quantities do not make sense on their own, so they need to be considered in a certain neighborhood.

Visual materials are frequently used in geomatics discipline. With the classification process applied to the remote sensing image, a digital classification map is obtained, and the classes are distinguished by pixel radiometric values. In a network adjustment, the confidence ellipses at the points forming the network can be drawn and the change of accuracy across the network can be visually presented. In detail surveys, the relationship between the points is recorded on a sketch in the field and this sketch forms the basis for map generation. Another important example of visualization is cartographic generalization, which is the process of combining details that would not normally be visible on their own in small-scale map production. The examples given above are selected examples that show that visualization activity constitutes an important part of cartography studies, and many more applications can be specified (Goudine et al., 2020; Lacey & Nelson, 2023; Liu et al. 2021; Yang et al., 2023; You et al., 2023; Zhang & Maram, 2025).

4. Results and Discussion

The point clouds obtained with M3C2 were utilized in the study. In order to use the point cloud with the highest accuracy within the scope of the study, it is important to evaluate it meticulously. Dense matching was carried out following the image matching and relative orientation phases, producing the orthophotos and point clouds that would be utilized in the study. The model's absolute orientation was established using ground control points (GCP), and independent control points (ICP) were used for model validation. GNSS relative positioning was used to determine the coordinates of the control points for each epoch, where network RTK was adopted for 3D coordinates of each control point. The standard deviations and root mean square errors obtained with GCPs and ICPs for all epochs are shown in Table 2. The accuracy values found with ICP are more acceptable than those found with GCP. They are consistent with the practical values of 0.25-0.5xGSD for the horizontal component and 0.5-1.0xGSD for the vertical component. The role of ICPs is central to this study because they have the function of making the proposed 3D test statistic more realistic.

The second step was the extraction of change vectors from the point clouds created by the photogrammetric method, the quality of which was each tested separately. The M3C2 algorithm was used here. For each of the points in reference epoch, the corresponding point in compare epoch was determined and thus the change vector was found. It should be emphasized that each point in reference epoch may not have a corresponding point in compare epoch, since image matching is used to determine the points, it should not be ignored that there may be a gap in compare epoch due to the lack of a match at the relevant location. In M3C2, the change vector is given with four parameters: the absolute value of the vector and the unit vector components in the coordinate components of the change direction.

Table 2. Each epoch's RMSE values

Epoch	Number of GCPs / ICPs	RMSE X (cm) GCPs / ICPs	RMSE Y (cm) GCPs / ICPs	RMSE Z (cm) GCPs / ICPs	Mean Ground Sampling Distance (GSD) (cm)
0	5/4	0.80 / 0.74	0.52 / 0.30	0.92 / 3.30	6.6
1	10/9	0.57 / 1.07	0.39 / 1.29	0.39 / 2.80	6.5
2	7/3	0.38 / 3.15	0.63 / 2.67	0.90 / 2.35	5.6
3	10/10	0.58 / 0.77	0.52 / 1.56	0.57 / 2.91	6.8
4	8/7	0.71 / 1.00	0.75 / 1.86	0.74 / 2.68	5.5
5	9/9	0.43 / 1.48	0.49 / 1.82	0.32 / 3.79	6.2
6	12/11	0.60 / 1.72	0.38 / 1.37	0.32 / 1.66	5.3
7	12/12	0.72 / 1.49	0.74 / 2.12	1.12 / 5.17	5.9
8	14/15	0.56 / 1.76	0.45 / 1.83	0.40 / 4.04	5.8
9	13/12	0.39 / 1.39	0.42 / 1.36	0.43 / 4.55	6.0

When evaluating with M3C2, the fine registration stage is skipped. At this stage, in order to perform fine registration, which is applied to increase the registration accuracy obtained with georeferencing, it is necessary to select the locations where there is no change from one epoch to another and evaluate with the help of these points. However, considering the fact that there may not be a region within the study area that can be classified as fixed, this step was not applied. Only the reference area generated by the GCPs in both epochs is taken as a basis here.

M3C2 calculates the change vector components for each point in the reference point cloud. In the output file it produces, the 3D change vector components from the reference point cloud to the corresponding point in the compare cloud are given as well as the standard deviation values at both endpoints of the calculated change vector extending in the normal direction. The standard deviation values at the endpoints are obtained with the help of the points of reference and compare clouds lying inside a cylinder of diameter d passed in the normal direction. Using the norm of the change vector and its standard deviation, the significance of the change vector is tested with the following equation:

$$T_{c,M3C2} = \frac{c}{\sigma_{c,M3C2}} \sim N\left(0,1,1 - {}^{\alpha}/_{2}\right) \quad (1)$$

In eq. (1), c is the change vector norm, $\sigma_{c,M3C2}$ the calculated standard deviation and $N(0,1,1-\alpha/2)$ the table value corresponding to the probability of error α for a standardized normal distribution. Using 95% confidence level, the test result for each location given in the M3C2 output file is presented to the user as a binary indicator within the same line. However, the standard deviation values used by M3C2 are an internal accuracy measure since they are calculated by deviations from the mean value using the points within a cylinder of diameter d. As external accuracy, GNSS observations can be utilized which are originally collected for the orientation of point clouds and their validation. To test whether the change vector is statistically significant, we use the 3D distance equation, which is the norm of the difference of the beginning and end point vectors, i.e. the 1st and 2nd epoch coordinates:

$$c = \sqrt{(x_2 - x_1)^2 + (y_2 - y_1)^2 + (z_2 - z_1)^2} \quad (2)$$

A differential equation is obtained by taking the derivatives of the stochastic variables

$$dc = -\frac{(x_2 - x_1)}{c}dx_1 + \frac{(x_2 - x_1)}{c}dx_2 - \frac{(y_2 - y_1)}{c}dy_1 + \frac{(y_2 - y_1)}{c}dy_2 - \frac{(z_2 - z_1)}{c}dz_1 + \frac{(z_2 - z_1)}{c}dz_2 \quad (3)$$

Here the coefficients in front of the variables denote the unit vector components in the normal direction. The normal unit vector components can be retrieved from the output file produced with the point cloud generated with M3C2 and the equation (3) can be written in more compact form as

$$dc = -n_x dx_1 + n_x dx_2 - n_y dy_1 + n_y dy_2 - n_z dz_1 + n_z dz_2. \quad (4)$$

Error propagation is applied to equation (4) by assuming that the output variables provided by M3C2 in each epoch are independent. Thus, the variance of the change vector norm is computed as

$$\sigma_c^2 = n_x^2(\sigma_{x1}^2 + \sigma_{x2}^2) + n_y^2\left(\sigma_{y1}^2 + \sigma_{y2}^2\right) + n_z^2(\sigma_{z1}^2 + \sigma_{z2}^2). \quad (5)$$

For the coordinate variances on the right side of the equation, the rmse values found with ICPs (Table 2) can be used. However, considering that the GNSS coordinates obtained with network RTK are also stochastic variables, a more realistic variance can be estimated by considering the variances in the horizontal and vertical components for TUSAGA-Aktif with $\sigma_{xy} = \pm 3\ cm, \sigma_z = \pm 5\ cm$ (Bakıcı, 2017).

$$\sigma_{cr}^2 = \sigma_c^2 + \sigma_{xy}^2 + \sigma_z^2 \quad (6)$$

Test statistic based on 3D change vector can be checked by

$$T = \frac{c^2}{3\sigma_{cr}^2} \sim F_{3,f_1+f_2,1-\alpha} \quad (6)$$

using Fisher distribution (Koch, 1999), where f_1 and f_2 denote the number of ICPs in the reference and compare point clouds and α=0.05 the probability of error. For values of the test statistic exceeding the Fisher distribution table value, the change vector is statistically different from zero. In this way, the non-zero positions of the M3C2 change vector, which reveals the change between the two epochs, can be revealed.

The significant change locations produced by M3C2 based on its internal accuracy measures can be compared with the external accuracy-based change locations proposed in this study. Figure 2 shows the locations where the change vector is significant according to the original results produced by M3C2. The figure clearly distinguishes between the excavation and the landslide areas. What is striking in the figure is that M3C2 labels almost the entire area as statistically significant change locations. On the other hand, proposed test statistic with realistic variance reveals change in much fewer locations given in Figure 3. The example presented in Figures 2 and 3 shows the change occurred from Epoch 4 to Epoch 5 and there is a time difference of 10 days between these two epochs (Table 1). If analyzed with the internal accuracy measures of M3C2, it would be inevitable to infer that a change occurred in a large part of the area within a short time frame of 10 days, as in Figure 2. When the drone images of both epochs were compared by visual inspection, no concrete evidence supported the situation depicted in Figure 2. Thus, it was qualitatively confirmed that the change shown in Figure 3 is the more realistic one.

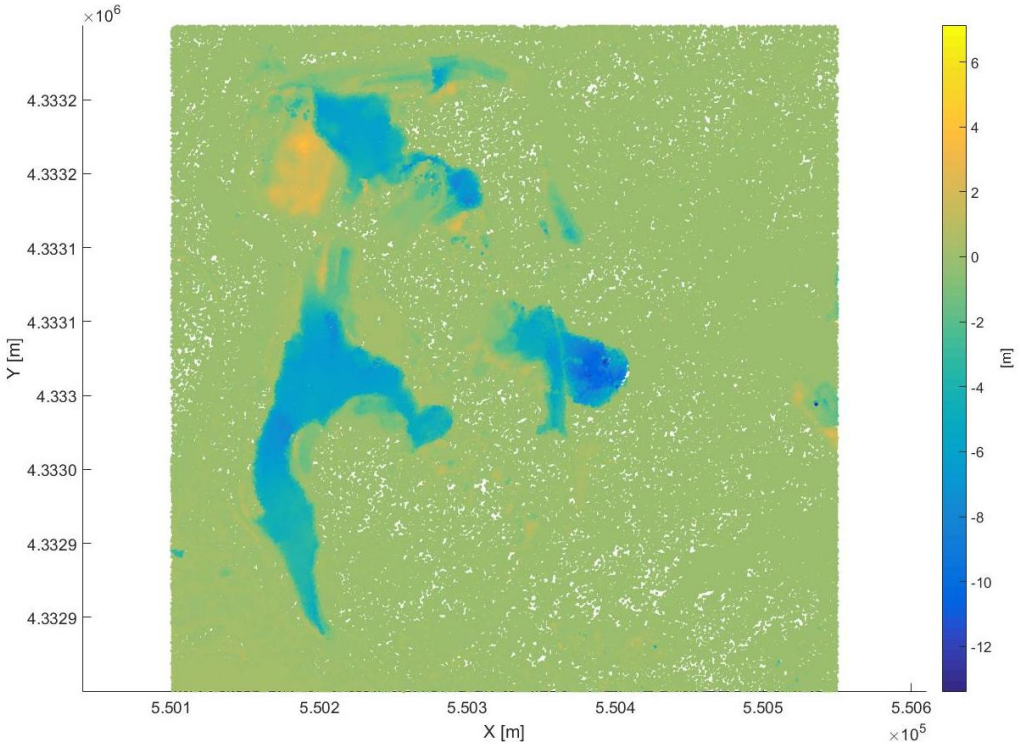

Figure 2. Change locations occurred between epoch4 – epoch5 revealed by M3C2's internal test statistic. The color scale shows the length of change vector where positive/negative values denote volume increase/decrease

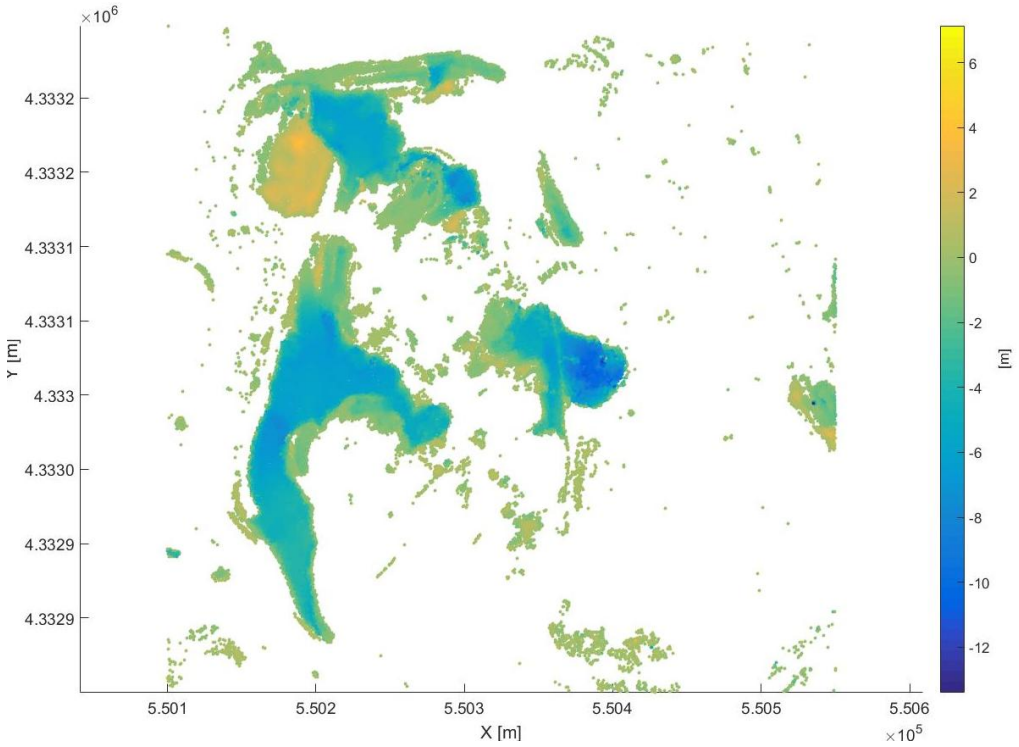

Figure 3. Same as Figure 2 but test statistic here is based on external accuracy values

Another example is the norms of the 3D and horizontal 2D change vectors detected in the area during the time interval Epoch 2 - Epoch 1. In Figure 4, a volume decrease can be seen in the area indicated by A and an increase in B. When the 3D and 2D changes are analyzed, it is easy to visually distinguish between the two regions, but an experienced interpretation is needed to reveal the nature of the change. As can be seen in Figure 5, A is an excavation and B a landslide area, it is likely that even the use of both visualizations together may lead an inexperienced user to erroneous interpretation. Here, visualization can be done with a new variable by transforming the M3C2 results. The ratio of the 2D change in xy-plane to the 3D change

$$c_{ratio} = \frac{c_{xy}}{c} \tag{8}$$

can be plotted for all points as in Figure 6. The ratio obtained by equation (8) is more useful for visually distinguishing between changes of different nature at locations A and B.

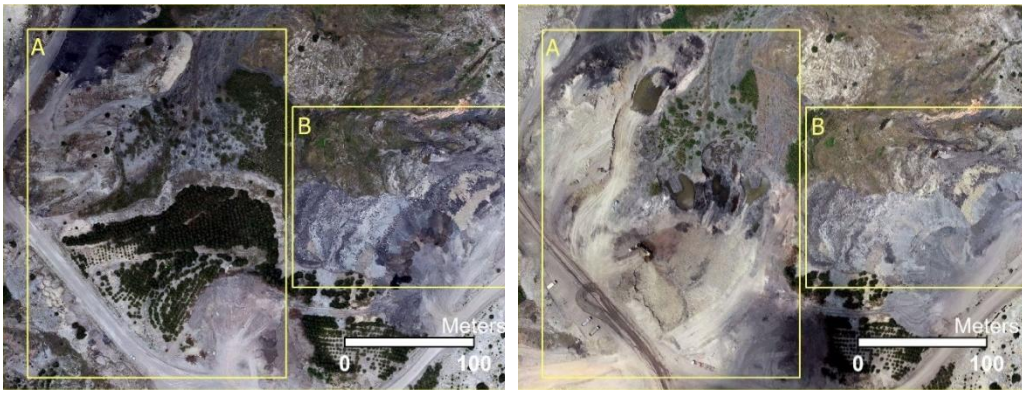

Figure 4. Close views of orthoimages bounded by rectangles A and B depicted Figure 1. (Left) Epoch 1 (30.05.2021) (right) Epoch 2 (23.06.2021) orthoimages

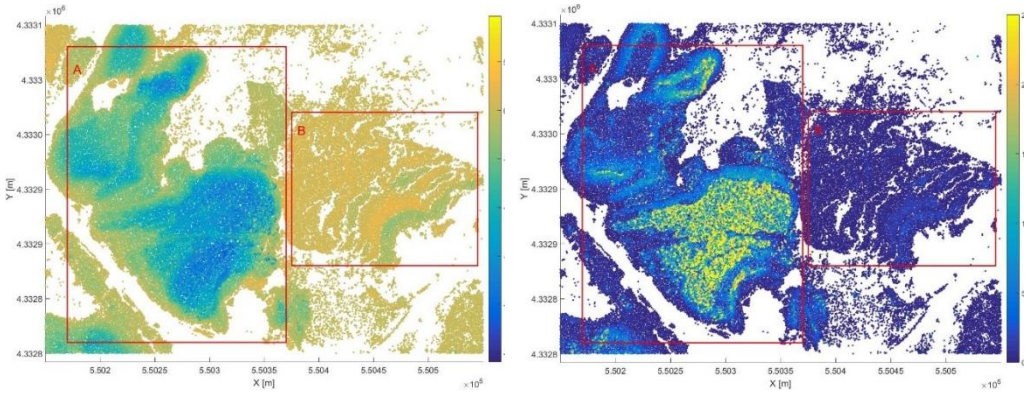

Figure 5. (Left) Significant 3D change vector length, (right) 2D change vector norm from epoch 1 (30.05.2021) to epoch 2 (23.06.2021)

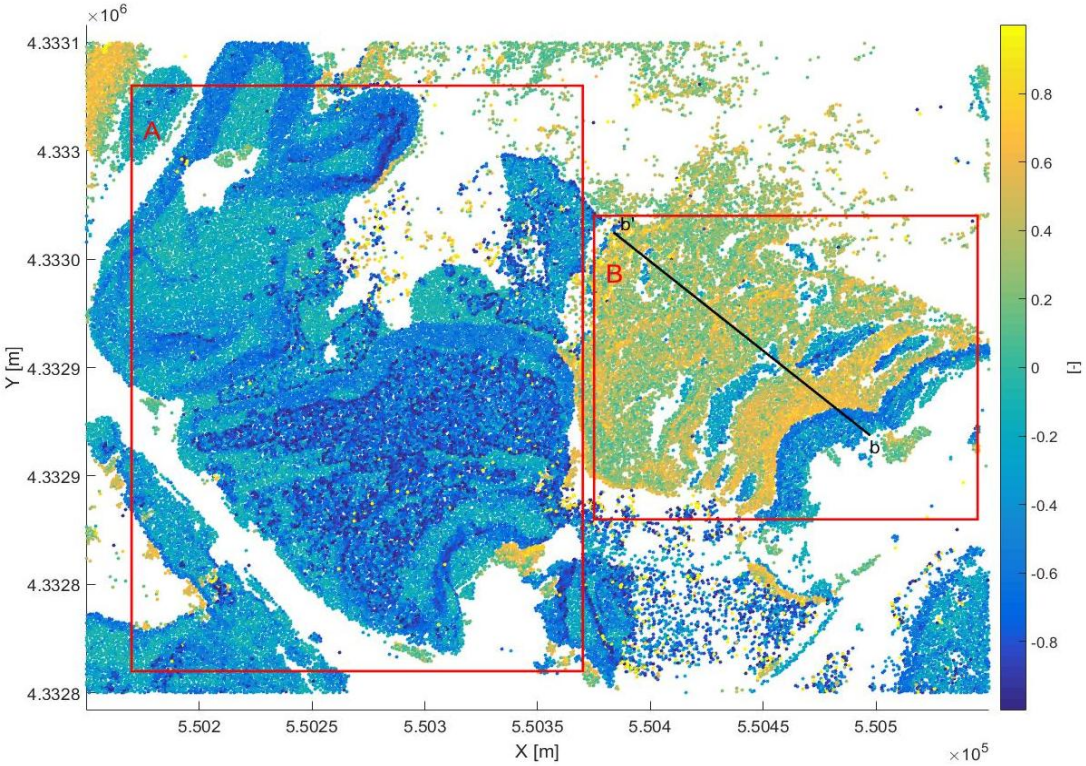

Figure 6. Ratio values for an excavation (A) and for a landslide (B) area. The extent of the area is the same as in Figures 4 and 5 but with a larger scale. bb' is a profile 147 m in length

In another location shown in Figure 7, the landslide movement between Epoch 8 and Epoch 9 can be difficult for the user to differentiate between 3D and 2D components as depicted in Figure 8's upper panel, whereas using a ratio allows the user to clearly identify the locations where horizontal movement is dominant (Figure 8).

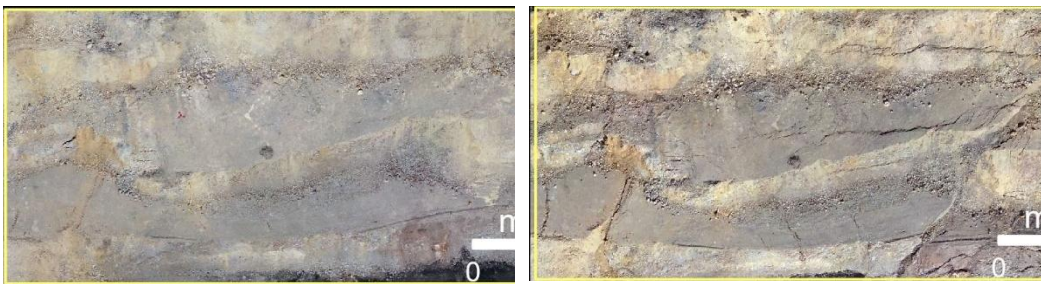

Figure 7. Close views of orthoimages bounded by rectangle C depicted Figure 1. (Left) extract of epoch 8 (15.04.2022) orthoimage, (right) extract of epoch 9 (19.10.2022) orthoimage

Two different profiles were used to observe the variation of the proposed ratio value against the changing topography between two epochs. DoD (DSM of Difference) values were interpolated along two selected lines (bb' and cc') with 1 m spacing (Figure 6 and Figure 8). The ratio values at the profile points were interpolated from the point cloud using the M3C2 outputs. Figure 9 shows the DoD values (blue) and the proposed ratio values (orange) for both profiles. In Figure 9a, it should be noted that DoD values are positive in the first 20m of the profile due to the storage of spoils in heap. In this 20 m section of the bb' profile, the ratio values are negative and the area around this portion of line is shown in turquoise and blue colors as can be seen in Figure 6. In the section between 20m and 50m of the profile, the DoD values are negative, and the ratio values vary between 0.4-0.6 as a result of the downward flow of the spoils in accordance with the slope of the heap. In Figure 6, the coloration of the ratio in the relevant section can be seen from light green to yellow. The ratio values beginning from 65 m to the end of profile (b') are mostly positive and around 0.4 on average. While 3.5 -4.0 m horizontal dislocations are observed at the head of the landslide, these values decrease to 2.5 m at its toe.

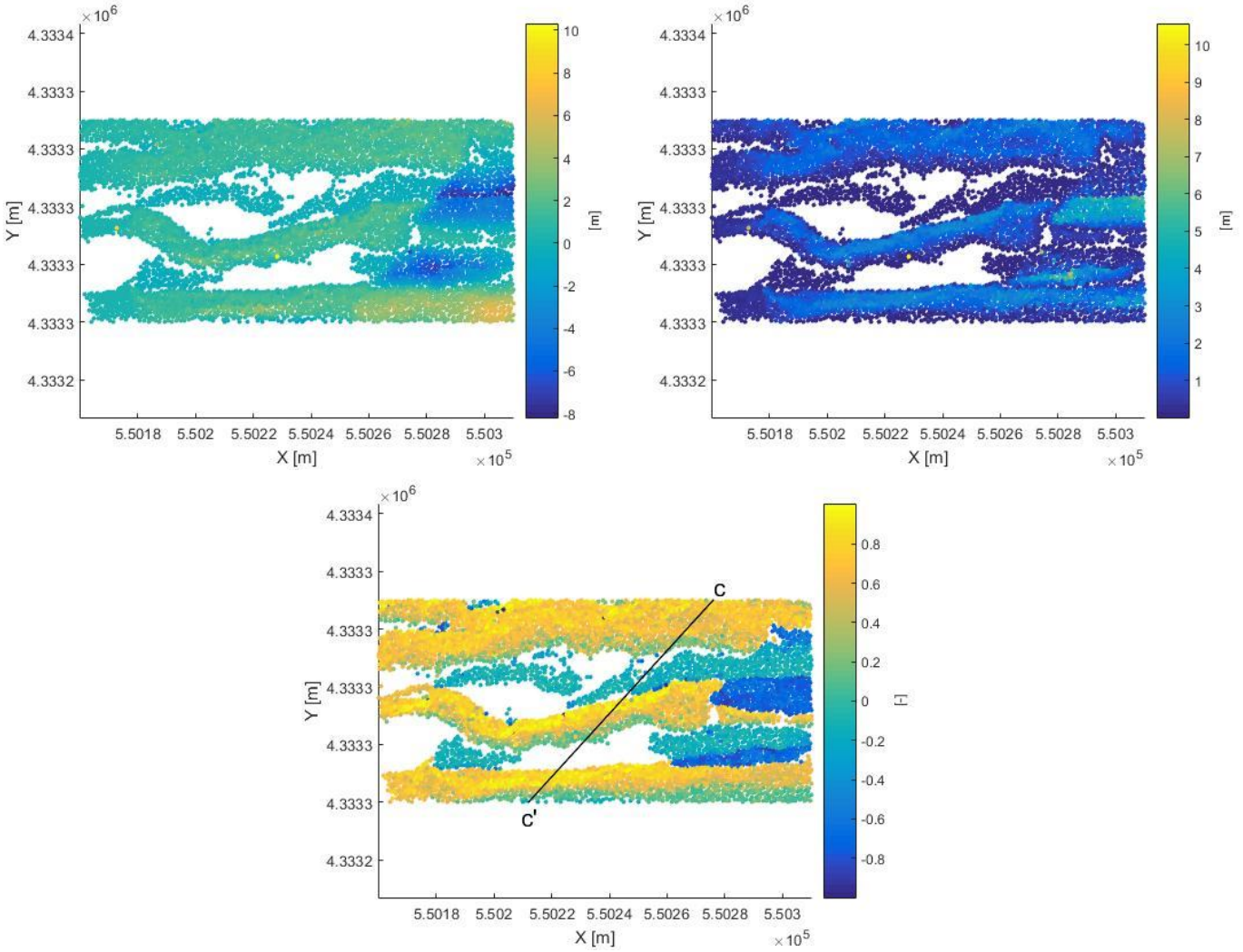

Figure 8. The extent of the area is the same as in Figure 7. (Upper left) significant 3D change vector length, (upper right) 2D change vector norm from epoch 8 (15.04.2022) to epoch 9 (19.10.2022), (below center) ratio values for the area. cc' is a profile 104 m in length

Figure 9b shows the variation of DoD and ratio values along the cc' profile given in Figure 8. Here, a clearer correspondence between the ratio and the horizontal movement caused by landslides is observed. In the areas bounded by rectangles in the figure, the

calculated ratio values are 0.7 and above. While 3.5-3.8 m displacements are observed at the head locations close to c in the profile, 3.3 m lateral displacements are observed at the toe. The direct use of M3C2 output produces optimistic results in revealing significant, non-zero significant change locations. Although it has been proposed to take into account registration error as well as variance for reference and compare points in the M3C2 method (Lague et al., 2013), the computed variance is still an optimistic measure based on internal accuracy of the solution. In this study, we propose to use a 3D test statistic with realistic accuracy values. Within the study, it is also emphasized that the ratio of 2D horizontal and 3D changes in a location is important in determining whether the change in that location is dominant in the horizontal direction. A larger ratio may be an important indicator for localizing movements such as landslides at the relevant location.

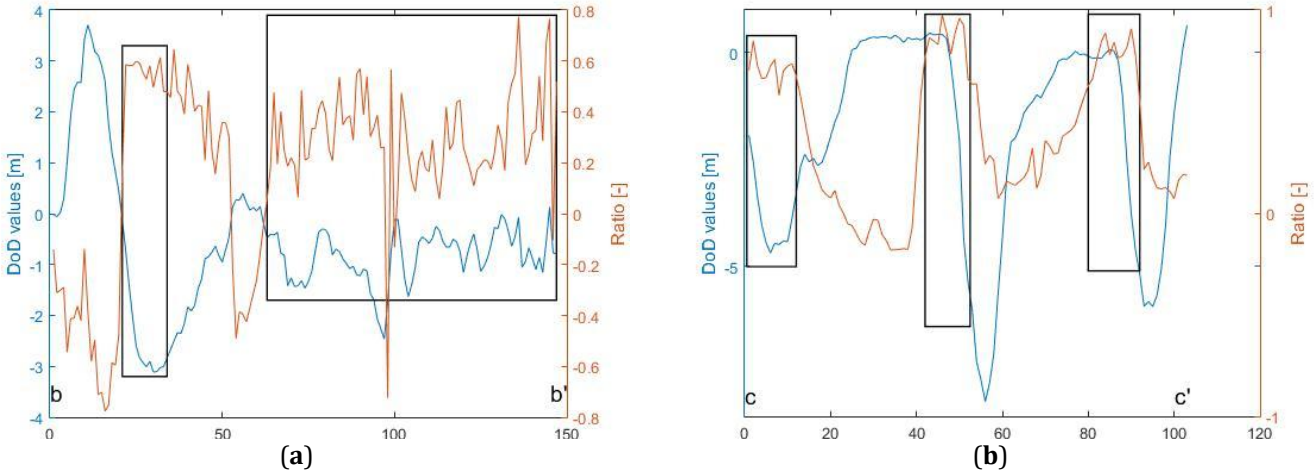

Figure 9. Variation of DoD and ratio values along the bb' and cc' profiles, depicted in Figures 6 and 8, respectively. The rectangles show profile sections having the highest positive ratio values and are identified as landslides

This study aims to visually highlight potential landslide areas with a metric derived from M3C2 outputs. So far, it has been a conventional approach to use the outputs for visual interpretation. Yan et al. (2024) combined M3C2 with other methods to analyze rainfall-induced slope changes and used visualization for qualitative validation of the results. In this study, a quantitative-based approach is proposed to identify potential areas. The proposed approach helps users to identify problem areas without straining their cognitive capacity. This can be especially important for applications under time pressure. It can be used to alleviate the pressure on the decision makers by directing their attention to the highlighted location. The quantitative-based visualization approach proposed in this study can also be used to test the results found with other analytical-based approaches. For example, our proposed method can be used as cross validation in a ML-based landslide area identification study.

Some limitations of the proposed approach should be emphasized. Control points obtained from GNSS observations are used to provide realistic accuracy values. In practice, if there are problems in obtaining such data or if there are not enough points with a suitable distribution in the field, there may be problems in obtaining realistic accuracy values. The proposed metric may also have some limitations in practice. For example, a high positive value indicates a dominant horizontal movement. The ratio values of a horizontal motion with a small change vector and a motion with a large change vector may be close to each other. In these cases, the absolute value of the motion should also be considered in the evaluations.

The study focuses on the identification of landslides due to excavations in an open pit mine site. It is important to test the study at other mine sites to provide independent tests.

The proposed approach can also be verified in other settings such as geomorphologically induced change and hazard situations as well as change in settlement areas. The conventional use of the metric proposed in this study can thus be investigated and the generalization of the method can be evaluated for several settings.

5. Conclusions

The importance of utilizing visual material is emphasized with the examples shown in the study. In monitoring studies consisting of a large number of points, visualization can be utilized by highlighting the necessary locations without straining the user's limited cognitive capacity. This is because visual material can support the decision maker in sudden decision-making situations that require rapid intervention. Visualization can also be used for validation of the results produced by machine learning and kinematic modeling methods used in slope stability studies. Here visualization can serve as a fast and economical tool for assessing the necessity of additional data across an area. For further confirmation, it may be possible to direct a drone to collect new data to locations upon quick visual assessment of the results.

In this study, an attempt has been made to answer the presented research question with the available data. The data used here are not the data obtained within the scope of any pre-planned project, but data collected in order to present to the responsible public institution by mapping the current change situations in the mine site with relatively economical photogrammetric method. As such, the present study has also an exploratory character together with its research questions. However, a research project aiming to collect data with appropriate temporal and spatial resolution to visualize landslide development in an open pit mine can be planned and implemented. In this way, it will be possible to develop a visualization model with realistically designed data.

Acknowledgments: The authors would like to express their sincere gratitude to FİDES Mühendislik for providing access to the UAV images used in this article, and to İzmir Katip Çelebi University for supplying the necessary computer hardware and software to analyze the data. The authors also gratefully acknowledge the anonymous reviewers for their insightful comments and constructive suggestions, which greatly contributed to improving the quality and clarity of the manuscript.

Author Contributions:

M. G. Koçak: Conceptualization, Methodology, Data processing, Writing—Original draft preparation, Reviewing and Editing.

N. Özdaş: Conceptualization, Methodology, Data processing, Writing—Original draft preparation, Reviewing and Editing.

O. S. Kırtıloğlu: Conceptualization, Methodology, Data processing, Writing—Original draft preparation, Reviewing and Editing.

Research and publication ethics statement: In the study, the author/s declare that there is no violation of research and publication ethics and that the study does not require ethics committee approval.

Conflicts of Interest: The authors declare no conflicts of interest.

References

Agisoft LLC. (2018). PhotoScan (Version 1.4) [Computer software]. Retrieved April 2, 2025, from https://www.agisoft.com/

Altiti, A. H., Alrawashdeh, R. O., & Alnawafleh, H. M. (2021). Open pit mining. Mining techniques-past, present and future. IntechOpen. https://doi.org/10.5772/intechopen.92208

Bakıcı, S. (2017, November 2-3). GNSS Reference Stations in Türkiye [Paper presentation]. Turkish National Geodetic Commission 2017 Scientific Meeting: Applications of GNSS Reference Stations, İstanbul, Türkiye.

Carrasco, M. (2011). Visual attention: The past 25 years. *Vision Research*, 51(13), 1484–1525. https://doi.org/10.1016/j.visres.2011.04.012

CloudCompare. (2020). CloudCompare (Version 2.12.2) [Computer software]. Retrieved April 2, 2025, from https://www.cloudcompare.org/

Cook, K. L. (2017). An evaluation of the effectiveness of low-cost UAVs and structure from motion for geomorphic change detection. *Geomorphology*, 278, 195–208. https://doi.org/10.1016/j.geomorph.2016.11.009

Goudine, A., Newell, R., & Bone, C. (2020). Seeing climate change: A framework for understanding visualizations for climate adaptation. *ISPRS International Journal of Geo-Information*, 9(11), 644. https://doi.org/10.3390/ijgi9110644

Hacıefendioğlu, K., Demir, G., & Başağa, H. B. (2021). Landslide detection using visualization techniques for deep convolutional neural network models. *Natural Hazards*, 109(1), 329–350. https://doi.org/10.1007/s11069-021-04838-y

He, H., Ming, Z., Zhang, J., Wang, L., Yang, R., Chen, T., & Zhou, F. (2024). Robust Estimation of Landslide Displacement from Multi-temporal UAV Photogrammetry-Derived Point Clouds. *IEEE Journal of Selected Topics in Applied Earth Observations and Remote Sensing*. https://doi.org/10.1109/JSTARS.2024.3373505

Intrieri, E., Carlà, T., & Gigli, G. (2019). Forecasting the time of failure of landslides at slope-scale: A literature review. *Earth-Science Reviews*, 193, 333–349. https://doi.org/10.1016/j.earscirev.2019.03.019

Jarrahi, M. H. (2018). Artificial intelligence and the future of work: Human-AI symbiosis in organizational decision making. *Business Horizons,* 61(4), 577–586. https://doi.org/10.1016/j.bushor.2018.03.007

Koch, K. R. (1999). Parameter estimation and hypothesis testing in linear models. Springer Science & Business Media.

Lacey, L. M., & Nelson, J. K. (2023). Using geovisual analytics to enrich conservation science: a review of interactive visualization of wildlife and environmental spatial data across ecosystems. *International Journal of Cartography*, 9(2), 286–318. https://doi.org/10.1080/23729333.2023.2190628

Lague, D., Brodu, N., & Leroux, J. (2013). Accurate 3D comparison of complex topography with terrestrial laser scanner: Application to the Rangitikei canyon (NZ). *ISPRS Journal of Photogrammetry and Remote Sensing,* 82, 10–26. https://doi.org/10.1016/j.isprsjprs.2013.04.009

Liang, R., Huang, C., Zhang, C., Li, B., Saydam, S., & Canbulat, I. (2023). Exploring the fusion potentials of data visualization and data analytics in the process of mining digitalization. *IEEE Access*, 11, 40608–40628. https://doi.org/10.1109/ACCESS.2023.3267813

Liu, H., Chen, X., Wang, Y., Zhang, B., Chen, Y., Zhao, Y., & Zhou, F. (2021). Visualization and visual analysis of vessel trajectory data: A survey. *Visual Informatics*, 5(4), 1–10. https://doi.org/10.1016/j.visinf.2021.10.002

Liu, X., Zhu, W., Lian, X., & Xu, X. (2023). Monitoring mining surface subsidence with multi-temporal three-dimensional unmanned aerial vehicle point cloud. *Remote Sensing*, 15(2), 374. https://doi.org/10.3390/rs15020374

MAPEG. (2025). Retrieved May 20, 2025, from https://www.mapeg.gov.tr/

Ospina-Dávila, Y. M., & Orozco-Alzate, M. (2020). Parsimonious design of pattern recognition systems for slope stability analysis. *Earth Science Informatics*, 13(2), 523–536. https://doi.org/10.1007/s12145-019-00429-5

Özdaş, N., Koçak, M. G., & Karakış, S. (2024). Examining the accuracy of DEM of difference and 3D point cloud comparison methods: Open pit mine case study. *Journal of Geodesy and Geoinformation*, 11(1), 41–50. https://doi.org/10.9733/JGG.2024R0004.E

Reichstein, M., Camps-Valls, G., Stevens, B., Jung, M., Denzler, J., Carvalhais, N., & Prabhat, F. (2019). Deep learning and process understanding for data-driven Earth system science. *Nature*, 566(7743), 195–204. https://doi.org/10.1038/s41586-019-0912-1

Ren, H., Zhao, Y., Xiao, W., & Hu, Z. (2019). A review of UAV monitoring in mining areas: Current status and future perspectives. *International Journal of Coal Science & Technology*, 6, 320–333. https://doi.org/10.1007/s40789-019-00264-5

Song, Z., Li, X., Huo, R., & Liu, L. (2024). Intelligent early-warning platform for open-pit mining: current status and prospects. *Rock Mechanics Bulletin,* 3(1), 100098. https://doi.org/10.1016/j.rockmb.2023.100098

Teng, J., Shi, Y., Wang, H., & Wu, J. (2022). Review on the research and applications of TLS in ground surface and constructions deformation monitoring. *Sensors*, 22(23), 9179. https://doi.org/10.3390/s22239179

Yang, Z., Li, J., Hyyppä, J., Gong, J., Liu, J., & Yang, B. (2023). A comprehensive and up-to-date web-based interactive 3D emergency response and visualization system using Cesium Digital Earth: taking landslide disaster as an example. *Big Earth Data*, 7(4), 1058–1080. https://doi.org/10.1080/20964471.2023.2172823

You, J., Zhu, J., Li, W., Guo, Y., Fu, L., & Dang, P. (2023). ROI-constrained visualization of flood scenes to improve perception efficiency. *International Journal of Digital Earth*, 16(1), 3065–3084. https://doi.org/10.1080/17538947.2023.2241430

Zhang, Q., & Maram, N. (2025). Multidimensional data visualization and synchronization for revealing hidden pandemic information. *Information Visualization*, 24(1), 95–113. https://doi.org/10.1177/14738716241277559